Vorticity gradient stretching in the direct enstrophy transfer process of two-dimensional turbulence

Zeyou Zhou
Center for Combustion Energy, Tsinghua University, Beijing 100084, China
and Department of Energy and Power Engineering, Tsinghua University, Beijing 100084, China

Lei Fang and Nicholas T. Ouellette
Department of Civil and Environmental Engineering, Stanford University, Stanford, California 94305, USA

Haitao Xu*
Center for Combustion Energy, Tsinghua University, Beijing 100084, China
and School of Aerospace Engineering, Tsinghua University, Beijing 100084, China

(Received 21 November 2019; accepted 8 April 2020; published 11 May 2020)

Vortex gradient stretching is believed to be the mechanism that generates large vorticity gradients at small scales and consequently maintains the enstrophy cascade to small scales in two-dimensional turbulence. In this work, using particle tracking measurements of two-dimensional turbulence in a soap-film flow, we show experimental evidence that in the direct enstrophy cascade range, the vorticity gradient is preferentially perpendicular to the instantaneous stretching direction. We also show that in regions where the stretching direction and the vorticity gradient are perpendicular to each other, the enstrophy flux is on average from large to small scales, while it is from small to large scales in other regions. Moreover, when observing the angle between stretching and the vorticity gradient in a coordinate system following a fluid particle trajectory, i.e., in the Lagrangian view, we observe that the vorticity gradient direction responds to but lags behind the stretching direction. Therefore, we observe a stronger alignment between the vorticity gradient direction with the stretching direction at an earlier time. At all scales in the direct cascade range, the evolution of the angle between the vorticity gradient and the stretching direction displays a time scale given by the mean enstrophy, independent of the scale, providing direct experimental support for the theoretical argument that vorticity is nearly constant in the direct cascade range.

DOI: 10.1103/PhysRevFluids.5.054602

I. INTRODUCTION

A primary feature of fluid turbulence is the net flux of kinetic energy from the scale where it is injected into the flow to the scale where it is dissipated. This energy flux over a wide range of scales is known as the energy cascade. In three-dimensional (3D) turbulent flows, vortex stretching, i.e., the average amplification of vorticity under the action of strain [1], is thought to play an important role in the cascade of energy from large scales to small scales [2–5]. In two-dimensional (2D) turbulence, vortex stretching is absent due to geometric constraints, and energy dissipation is dominated by large-scale friction. This difference leads to a transfer of energy from the forcing scale to larger scales known as the inverse energy cascade [6,7].

*hxu@tsinghua.edu.cn

 ©2020 American Physical Society

Another feature of 2D turbulence can be seen from the equation of motion for the enstrophy (that is, one half of the mean squared vorticity, $\langle \frac{1}{2}\omega^2 \rangle$) in a homogeneous field, given by [5]

$$\frac{1}{2}\frac{D\langle \omega^2 \rangle}{Dt} = \langle \boldsymbol{\omega} \cdot \nabla \times \mathbf{f} \rangle - \nu \langle (\nabla \omega)^2 \rangle - \alpha \langle \omega^2 \rangle, \tag{1}$$

where the angle brackets $\langle \cdot \rangle$ denote an ensemble average; $\boldsymbol{\omega} = \omega \mathbf{e}_z$ is the vorticity vector, which is normal to the 2D plane of the flow; $\mathbf{f}$ is the external force in the plane of the flow; ν is the kinematic viscosity of the fluid; and α is a friction coefficient that characterizes the large-scale drag. The first term on the right-hand side of this expression is the rate of enstrophy injection by external forces, which acts at the forcing scale L_F. The second term is the rate of enstrophy dissipation by viscosity, $\beta \equiv \nu \langle (\nabla \omega)^2 \rangle$, which becomes significant at the dissipative scale $\eta \equiv \nu^{1/2}/\beta^{1/6}$. The third term is the rate of enstrophy dissipation due to large-scale friction, which primarily contains contributions from scales in the range from L_F up to $L_\alpha \equiv (\varepsilon/\alpha^3)^{1/2}$, where $\varepsilon = \alpha \langle u^2 \rangle$ is the energy dissipation rate and L_α is the scale at which friction arrests the inverse energy cascade. Standard analysis [7] leads to $L_F/\eta \sim \mathrm{Re}_\omega^{1/2}$ and $L_\alpha/L_F \sim \mathrm{Re}_\alpha^{3/2}$, with $\mathrm{Re}_\omega \equiv \omega' L_F^2/\nu$ and $\mathrm{Re}_\alpha \equiv (L_\alpha/u')/(\omega')^{-1} = \omega' L_\alpha/u'$, where $\omega' \equiv \langle \omega^2 \rangle^{1/2}$ and $u' \equiv \langle u^2 \rangle^{1/2}$ are the vorticity and velocity fluctuations. At large Reynolds numbers, $\mathrm{Re}_\omega \gg 1$ and $\mathrm{Re}_\alpha \gg 1$, the length scales are well separated and $\eta \ll L_F \ll L_\alpha$. Moreover, in that case, the contribution to the enstrophy dissipation from large-scale friction is negligible compared to the viscous dissipation as $\alpha \langle \omega^2 \rangle/\beta \sim \mathrm{Re}_\alpha^{-1}$. Therefore, at steady state, there must be a flux of enstrophy from the forcing scale to the dissipative scale, i.e., in the range $\eta \ll l \ll L_F$. In this direct cascade of enstrophy, the value of the enstrophy flux must be the same as the enstrophy dissipation rate β. This flux of enstrophy across scales is very similar to the energy cascade in 3D turbulence and has been predicted theoretically [8] and observed in experiments and numerical simulations [5,9–11].

For unforced 2D flows, the average enstrophy will decay as given by Eq. (1). When the viscosity is small, the decay is very slow and the above analysis still approximately holds, and the scale L_F, which now corresponds to the scale where the direct enstrophy cascade starts, is determined by the initial flow condition before the decay. In this case, both the scale L_F and η vary with time as the flow decays, though a net enstrophy flux from scale L_F to η is still present as long as there is still scale separation between the two, i.e., when $\mathrm{Re}_\omega \gg 1$.

The physical mechanism that leads to this flux of enstrophy must be consistent with the generation of vorticity gradients to maintain the viscous dissipation, as shown by Eq. (1). This is also analogous to the energy cascade in 3D turbulence, where the stretching of velocity gradients is believed to be the mechanism for the transfer of energy to small scales as it amplifies the energy dissipation at small scales by viscosity. For 2D turbulence, this leads to *vorticity gradient stretching*, since for unforced flows [5,8]

$$\frac{1}{2}\frac{D\langle (\nabla \omega)^2 \rangle}{Dt} = -\langle s_{ij} (\nabla \omega)_i (\nabla \omega)_j \rangle - \nu \langle (\nabla^2 \omega)^2 \rangle. \tag{2}$$

This expression is actually the balance equation for the mean palinstrophy, as palinstrophy, $\frac{1}{2}(\nabla \times \boldsymbol{\omega})^2$, reduces to $\frac{1}{2}(\nabla \omega)^2$ in 2D. In Eq. (2), the first term on the right-hand side represents vorticity gradient stretching (VGS), which captures the contribution to the change of the magnitude of vorticity gradient by the rate of strain tensor $s_{ij} = \frac{1}{2}(\partial_j u_i + \partial_i u_j)$. The VGS term can generate large vorticity gradients that help to maintain strong palinstrophy and consequently finite enstrophy dissipation even in the limit of vanishingly small viscosity. This, together with the enstrophy balance equation, Eq. (1), allows a flux of enstrophy from the scale L_F to the dissipative scale η. As a consequence of VGS, one would expect that the vorticity gradient would preferentially be perpendicular to the stretching direction, which has indeed been observed in numerical simulations [12]. On the other hand, as vorticity is not a passive scalar, it can affect the orientation of the gradient of a scalar, including the vorticity gradient itself [13]. This effect may alter the expected orthogonality between the stretching direction and the vorticity gradient [14,15]. This physics is different from the alignment between vorticity and the stretching direction in 3D, where the vorticity

does not rotate the direction of the vorticity vector itself, and hence this direct effect does not occur (but, note that even in that case, there are important differences between vorticity, a dynamical quantity, and a passive vector such as an infinitesimal material line [16]). Therefore, it is of interest to examine whether, in 2D turbulence, the vorticity gradient stretching, which is based on simple kinematic arguments, is still manifest in geometric statistics such as the angle between the stretching direction and the vorticity gradient direction.

In this work, we examine the connection between VGS and enstrophy flux at different scales in the direct enstrophy cascade range of a turbulent soap-film flow. By measuring the motion of micron-sized tracer particles seeded in the flow, we obtain the instantaneous velocity fields, on which we perform spatial filtering to extract the scale-dependent rate of strain fields and vorticity fields. We observe that in the direct enstrophy cascade range, on average, the vorticity gradient tends to be perpendicular to the stretching direction of the rate of strain field. In regions where the vorticity gradient and the stretching direction are close to perpendicular, the conditional mean of the enstrophy flux is from large to small scales, while this conditional mean is from small to large scales in other regions. Furthermore, as we obtain fluid particle trajectories, we probe the filtered vorticity field and the rate of strain field along these trajectories, i.e., in a Lagrangian view. In that coordinate system, we can observe the process of the vorticity gradient direction turning away from the stretching direction. The evolution time of this process shows interesting scale dependence that is consistent with the dynamical time scale of the turbulence in the direct enstrophy cascade range.

II. EXPERIMENTAL METHODS

The 2D turbulence data that we used came from laboratory experiments using a flowing soap film driven by gravity and confined within a 2D tunnel created by two nylon wires under tension, a setup that has been widely used in 2D turbulence studies [7,17–19]. As shown in Fig. 1, the soap solution flows from the upper reservoir into a nozzle, speeds up due to gravity in an expanding section whose length is $X_1 = 106$ cm, and then reaches an almost fully developed state in the measurement section of length $X_2 = 194$ cm and width $w = 5$ cm. The solution then enters the lower reservoir, where a peristaltic pump brings the solution back into the upper reservoir to complete the cycle. By adjusting the flow rate of the pump, the mean velocity of the soap film in the measurement section can be varied from 1 to 3 m/s and the film thickness from 4 to 9 μm. At a given pump speed, the mean film velocity changes by only 2% within the measurement section over a distance of 45 cm from the entrance of the straight section, and the mean velocity profile is nearly flat in the central 3 cm of the film at any cross section. Turbulence is created by inserting an array of equally spaced round rods into the film. The diameter of the rods is 1.14 mm and the spacing between the rods is $M = 5$ mm. Measurements were performed at distances of $20M$–$40M$ downstream of the rod array. The soap solution consisted of 2% Dawn detergent, 10% glycerol, and 88% deionized water, all by weight. The recipe has been tested many times before and the resulting soap films are stable and easy to handle [18,19].

We performed particle tracking to obtain quantitative measurements of the flow field. For that purpose, the soap solution was seeded with polystyrene spheres with a diameter of 1 μm manufactured by Duke Scientific. Since the thickness of the soap film before inserting the rod array was between 4 and 9 μm, as measured from interference fringes, the motion of the polystyrene spheres was not affected by the surfaces and thus they can be regarded as fluid tracers. The motion of these tracer particles was recorded by two high-speed cameras (Phantom VEO640L from Vision Research, Inc.), which were arranged such that their fields of view overlap in the streamwise direction and hence provided a large measurement area of 100×12 mm^2 in the middle of the flowing soap film. The frame format of the cameras was set to $(2\times)2560 \times 472$ pixels, which gave a spatial resolution of approximately 10 μm/pixel. The effective viscosity of the soap film was estimated to be $\nu = 6.5 \times 10^{-6}$ m^2/s by the empirical relationship between the Reynolds number and the Strouhal number of the Kármán vortex street behind a cylinder inserted in the soap

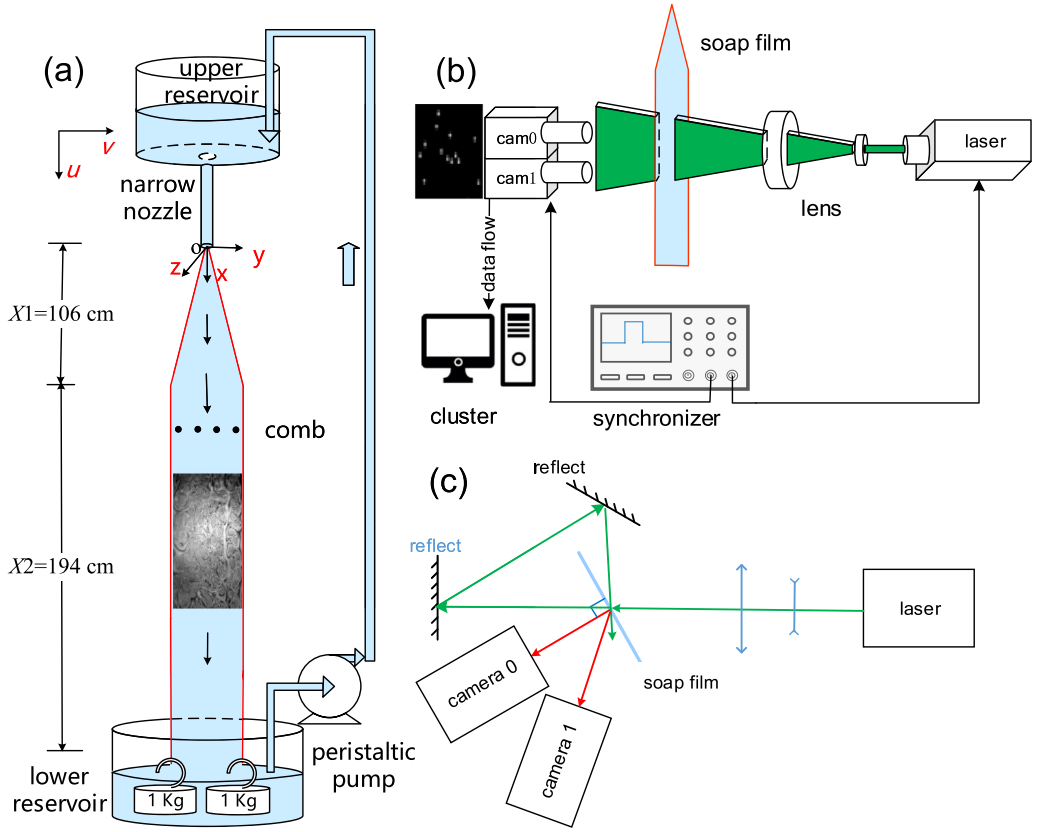

FIG. 1. The experimental setup. (a) The soap-film flow. The soap-film tunnel consists of two nylon wires with diameters of 0.32 mm held by hooks and weights. (b) A high-power, high-repetition-rate pulsed laser was used to illuminate tracer particles (1 μm in diameter) seeded into the soap solution, and two high-speed cameras were used to perform particle tracking measurements at different downstream locations. (c) Top view of the setup. The second camera was arranged at an angle to the soap film in order to ensure that the imaging fields from the two cameras overlapped.

film [20]. The enstrophy dissipation scale $\eta = \nu^{1/2}/\beta^{1/6}$ was about 0.33 mm in the measurement region, much larger than the spatial resolution of the measurement. Thus, the velocity field was well resolved. The camera frame rate was 5000 frames per second, which was also the repetition rate of the pulsed Nd:YAG laser. The laser and the two cameras were synchronized by an external signal.

After the images were taken, we used a particle tracking algorithm to find particle positions and track them in time to obtain Lagrangian trajectories of individual tracer particles [21]. Special care was taken in dealing with the overlap region between the two cameras, in which the consistency of both the particle position and the velocity were considered when matching trajectories observed in the overlap region, a technique that has been proposed and implemented successfully in solving similar problems [22,23]. With these particle trajectories, velocities and accelerations (if needed) of the tracers can be obtained by differentiation. As we observed many hundreds of tracer particles in each camera at any instant, Eulerian statistics such as velocity structure functions and spectra can also be obtained.

In the region where the measurements were performed, the average turbulent fluctuation velocity is $u' \approx 0.31$ m/s, and the average energy dissipation rate, measured from the decay rate of

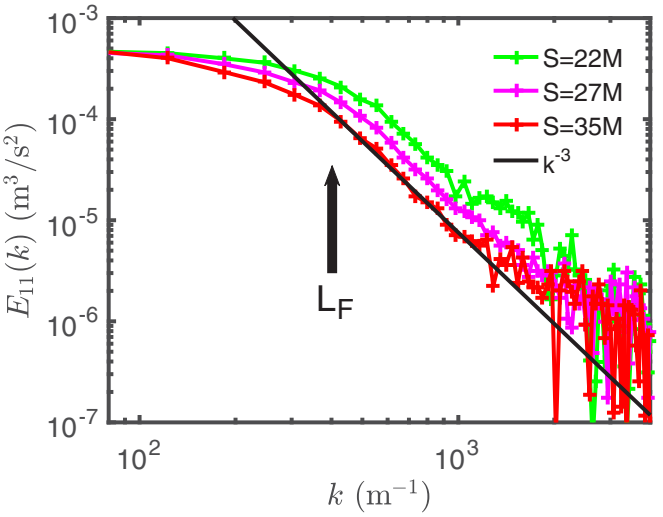

FIG. 2. Energy spectra measured at different positions in the observation area $20 < x/M < 40$ downstream of the rod array. All spectra show a developed k^{-3} range, which indicates a direct enstrophy cascade, and a short $k^{-5/3}$-like range. The effective forcing length scale L_F corresponds to the transition scale between these two regimes and grows as the flow moves downstream due to the decay of the turbulence.

the turbulent kinetic energy, is $\varepsilon \approx 0.9\ \mathrm{m}^2/\mathrm{s}^3$, which gives the average friction factor as $\alpha = \varepsilon/u'^2 \approx 9\ \mathrm{s}^{-1}$. The length scale at which friction dominates is thus $L_\alpha \equiv u'/\alpha \approx 34$ mm. The enstrophy dissipation rate β is determined from the scaling of the third-order Eulerian velocity structure function in the enstrophy cascade range given by $\langle[\delta_L u(r)]^3\rangle = \frac{1}{8}\beta r^3$, where $\delta_L u(r)$ is the longitudinal velocity increment [5], which gives $\beta \approx 1.7 \times 10^5\ \mathrm{s}^{-3}$. This value of β gives $\beta^{1/3} \approx 55\ \mathrm{s}^{-1}$, comparable to the average rms vorticity in the measurement region ($\omega' \approx 160\ \mathrm{s}^{-1}$) as suggested by the dimensional argument $\omega' \sim \beta^{1/3}$. The enstrophy dissipation scale is thus $\eta \equiv \nu^{1/2}/\beta^{1/6} \approx 0.33$ mm. The effective forcing scale L_F is on the order of the rod spacing M. (It may also be on the order of the rod diameter, but that is itself on the order of M.) For a decaying flow such as our soap film, we define L_F as the scale at which the scaling of the second-order structure function changes from $\langle[\delta_L u(r)]^2\rangle \sim \beta^{2/3} r^2$ to $\sim \varepsilon r^{2/3}$, which gives $L_F \equiv (\varepsilon/\beta)^{1/2} \approx 2.3$ mm in the measurement region. With these parameters we can calculate the Reynolds numbers defined in the introduction to be $\mathrm{Re}_\omega \approx 130$ and $\mathrm{Re}_\alpha \approx 18$. Note that these two Reynolds numbers directly characterize scale separations. Both $\mathrm{Re}_\omega \gg 1$ and $\mathrm{Re}_\alpha \gg 1$, indicating that there are wide scale separations between the friction scale L_α, the effective forcing scale L_F, and the dissipation scale η, as can be seen directly from $L_\alpha/L_F \approx 15$ and $L_F/\eta \approx 7$. Therefore, we conclude that the effect of the decay of the turbulent kinetic energy by large-scale friction on VGS, which occurs in the enstrophy cascade range, is negligible.

As the turbulence decays with the downstream position from the rods, both ε and β decrease. We observe the decrease of ε to be slower in our flow, likely due to the somewhat weaker frictional effect as indicated by the small value of α. Therefore, the effective forcing scale $L_F = (\varepsilon/\beta)^{1/2}$ increases as the flow moves downstream. Figure 2 shows measured energy spectra at different downstream positions. All the spectra show a k^{-3} regime, and the scale L_F, at which the k^{-3} regime changes to a shallower, $k^{-5/3}$-like, regime, shifts to larger scales as the flow moves downstream. This increase of L_F is moderate—less than a factor of 2 over the measurement regime. Moreover, there may be a constant of order unity between the value of L_F that we define as $L_F \equiv (\varepsilon/\beta)^{1/2}$ and the true effective forcing length scale. We therefore take $L_F \sim M$ in this work as a leading-order estimate of that scale.

III. EULERIAN OBSERVATIONS

To investigate the connection between vorticity gradient stretching and enstrophy flux at different scales, we utilized a filter-space technique, which is implemented in real space by convolving a kernel function that acts as a low-pass filter in Fourier space with a corresponding cutoff length scale r in real space [24–28]. The filtering is performed at a single time instant and on any region larger than or equal to the filter size r. Hence, it allows us to probe local scale-dependent quantities, such as the enstrophy flux, at any instant. In the rest of the paper, we use symbols with a superscript "$^{(r)}$" to represent filtered quantities, where r is the length scale of the filter.

The scale-dependent vorticity gradient stretching term corresponding to that in Eq. (2) is obtained from the filtered rate of strain and the filtered vorticity gradient as

$$G^{(r)} = -s_{ij}^{(r)}(\nabla\omega)_i^{(r)}(\nabla\omega)_j^{(r)} = -2\lambda_s^{(r)}\lambda_{\nabla\omega}^{(r)}\cos 2\Theta_{s\nabla\omega}^{(r)} = -\lambda_s^{(r)}|(\nabla\omega)^{(r)}|^2\cos 2\Theta_{s\nabla\omega}^{(r)}, \tag{3}$$

where $\lambda_s^{(r)}$ and $\lambda_{\nabla\omega}^{(r)}$ are the positive eigenvalues of the filtered rate of strain tensor $s_{ij}^{(r)}$ and the traceless part of the dyad formed by the filtered vorticity gradient $(\nabla\omega)_i^{(r)}(\nabla\omega)_j^{(r)}$, respectively, and $\Theta_{s\nabla\omega}^{(r)}$ is the angle between the eigenvectors $\mathbf{e}_s^{(r)}$ and $\mathbf{e}_{\nabla\omega}^{(r)}$ that correspond to $\lambda_s^{(r)}$ and $\lambda_{\nabla\omega}^{(r)}$, respectively. In the last equality of Eq. (3), we make explicit use of the relationship $2\lambda_{\nabla\omega}^{(r)} = |(\nabla\omega)^{(r)}|^2$. When $\pi/4 < \Theta_{s\nabla\omega}^{(r)} \leqslant \pi/2$, i.e., when the filtered vorticity gradient is close to perpendicular to the stretching direction of the filtered strain (in other words, nearly aligned with the most compressive direction of the strain), Eq. (3) shows that $G^{(r)} \geqslant 0$, which means that locally there is palinstrophy production by VGS and, consequently, that the vorticity gradient is amplified. This effect can also be explained by invoking the conservation of vorticity along a material line when viscosity is negligible; then, the packing of material lines under compression would result in an increase of the local vorticity gradient [26]. When $0 \leqslant \Theta_{s\nabla\omega}^{(r)} \leqslant \pi/4$, the opposite is true: the vorticity gradient is nearly aligned with the stretching direction of the strain, and the vorticity gradient will be weakened. Therefore, $\cos 2\Theta_{s\nabla\omega}^{(r)}$ may be regarded as an efficiency for the VGS: it quantifies the fraction of the strain rate that acts to amplify the vorticity gradient and hence to produce palinstrophy [29,30].

From this analysis, one would expect that in the direct enstrophy cascade range, the vorticity gradient should be preferentially perpendicular to the stretching direction of the rate of strain as a consequence of VGS. Figure 3 shows the probability density function (PDF) of the angle $\Theta_{s\nabla\omega}^{(r)}$ at different scales r in the direct enstrophy cascade range ($\eta \lesssim r \lesssim M$). If the two vectors were independent, the PDF would be a horizontal line. Data from our measurements instead show that there is preferential misalignment at all scales investigated and that the degree of misalignment is weaker as the scale increases. As discussed earlier, the effective forcing scale L_F grows with downstream distance [31,32], so that there is still appreciable alignment at scales above the initial forcing scale M. Both the antialignment and the change with scale have been reported before in direct numerical simulations (DNS) of forced 2D turbulence with periodic boundary conditions at steady state [12]. The agreement with our experiment using decaying turbulence indicates that VGS is ubiquitous in 2D turbulence.

Next, we investigate the connection between VGS and enstrophy flux. The enstrophy flux from scales larger than r to scales smaller than r is given by [33]

$$Z^{(r)} = -\left[(u_i\omega)^{(r)} - u_i^{(r)}\omega^{(r)}\right]\frac{\partial\omega^{(r)}}{\partial x_i}. \tag{4}$$

A positive value of $Z^{(r)}$ means that at the instant of time measured, enstrophy is locally being transferred down to smaller scales (i.e., an instantaneously direct enstrophy flux). In Fig. 4(a), we plot the mean enstrophy flux $\langle Z^{(r)}\rangle$ at different scales. Note that the enstrophy flux obtained from the filtering technique is smaller than that estimated from the third-order velocity structure function, as observed in the literature [32]. It is indeed positive at all scales investigated. In the same plot, we also show the mean enstrophy flux conditioned on being in a VGS region (where $\Theta_{s\nabla\omega}^{(r)} > \pi/4$) and in a non-VGS region (where $\Theta_{s\nabla\omega}^{(r)} < \pi/4$). In VGS regions, the conditional mean of the

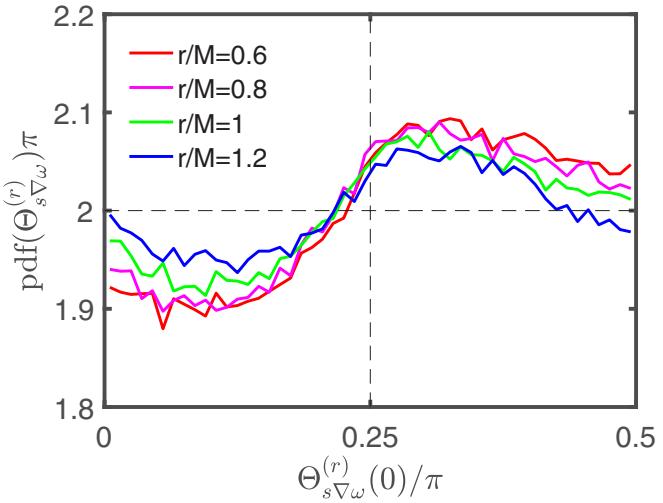

FIG. 3. PDF of the angle between the filtered vorticity gradient and the stretching direction of the filtered rate of strain at different scales in the direct enstrophy cascade range, which corresponds to $\eta \lesssim r \lesssim M$ (as seen in the energy spectrum).

enstrophy flux is positive and its value is considerably larger than the unconditional mean, while the conditional mean is negative in non-VGS regions. This result shows that VGS is tightly related to the enstrophy flux. For comparison, we also plotted the mean enstrophy flux conditioned on being in a strain-dominated region (where the parameter $Q \equiv \omega^2/2 - s^2 < 0$) and in a vorticity dominated region ($Q > 0$). These conditional means are nearly the same as the unconditional mean, which shows that the magnitude of the stretching alone does not determine the direction of the enstrophy

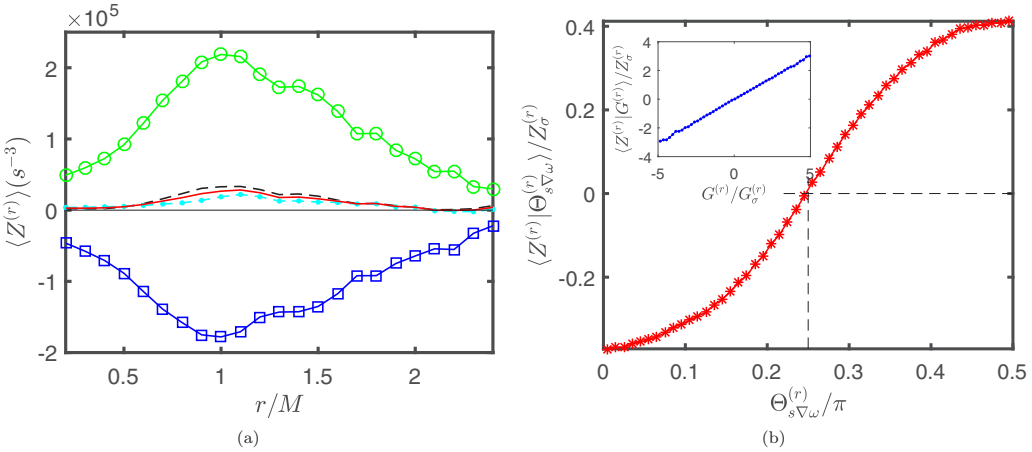

FIG. 4. (a) Mean filtered enstrophy fluxes $\langle Z^{(r)}\rangle$ as a function of scale r. Red solid line, unconditional mean; green circles, conditional mean in VGS regions ($\Theta^{(r)}_{s\nabla\omega} > \pi/4$); blue squares, conditional mean in non-VGS regions ($\Theta^{(r)}_{s\nabla\omega} < \pi/4$); black dashed line, conditional mean in strain-dominated regions ($Q < 0$); and cyan dot-dashed line, conditional mean in vorticity-dominated regions ($Q > 0$). (b) Mean enstrophy flux $\langle Z^{(r)}\rangle$ conditioned on the angle between the vorticity gradient and the stretching direction at scale $r = 0.8M$. The inset shows $\langle Z^{(r)}\rangle$ conditioned on the value of the VGS $G^{(r)}$. $Z^{(r)}$ and $G^{(r)}$ are normalized by their standard deviations $Z^{(r)}_\sigma$ and $G^{(r)}_\sigma$, respectively.

flux. A direct calculation of $\langle Z^{(r)}|Q\rangle$ (not shown) gives the same conclusion. In Fig. 4(b), we plot the mean enstrophy flux conditioned on $\Theta^{(r)}_{s\nabla\omega}$, the angle between the vorticity gradient and the stretching direction of the strain, at the scale $r = 0.8M$. The conditional mean grows monotonically with the angle $\Theta^{(r)}_{s\nabla\omega}$. In the inset, we show the mean enstrophy flux conditioned on the vorticity gradient stretching $G^{(r)}$, which shows a remarkable straight line. Similar behavior was observed for other scales r. This strong connection between VGS and enstrophy flux was also observed in direct numerical simulations and the linear dependence between $\langle Z^{(r)}\rangle$ and $G^{(r)}$ also motivated a closure model for $Z^{(r)}$ [12].

IV. LAGRANGIAN ALIGNMENT

In Fig. 3, we see that there is a preferential misalignment between the vorticity gradient direction and the stretching direction due to VGS. This misalignment, however, is rather weak, which leads to significant cancellation of local positive and negative fluxes and therefore only a weakly positive net value of the enstrophy flux [see Fig. 4(a)]. This weak alignment is reminiscent of the case of vortex stretching in 3D turbulence. There, it is expected on physical grounds that vorticity itself should be preferentially aligned with the most stretching direction of the rate of the strain due to vortex stretching. Numerical simulations and experimental data show, however, that surprisingly vorticity is preferentially aligned with the intermediate eigenvector of the strain, leading to rather weak net stretching [34,35]. This poor alignment of instantaneous quantities can be partially understood by considering dynamic effects. The strain field indeed can stretch the vorticity, which causes the vorticity to grow in the direction of stretching; but the strain field itself changes with time, and hence only a weak alignment between vorticity and strain is found when observing at any instant. To demonstrate the vortex stretching effect, one must examine the vorticity evolution in a fixed eigenframe of strain along a Lagrangian trajectory [36,37] or in a fully Lagrangian formulation [38]. This work motivated us to investigate the change of the angle between the vorticity gradient and the stretching direction in the eigenframe of the strain. However, we note that in 2D the direction of the vorticity gradient can be changed by vorticity itself, as we will see later more explicitly. This is different from the 3D case, where the direction of the vorticity vector is not rotated by the vorticity directly.

Inspired by studies of vortex stretching in 3D, we computed the alignment between the vorticity gradient and the strain rate in a frame following a Lagrangian trajectory. In particular, we calculated the angle between the vorticity gradient and the stretching direction with a time lag: $\Theta^{(r)}_{s\nabla\omega}(t) = \cos^{-1}[\mathbf{e}^{(r)}_{\nabla\omega}(t)\cdot\mathbf{e}^{(r)}_{s}(0)]$. In Fig. 5(a), we plot the evolution of the average angle $\langle\Theta^{(r)}_{s\nabla\omega}(t)\rangle$ with time for different scales r, which quantifies the (anti)alignment of the vorticity gradient with the stretching direction in the eigenframe of the earlier strain. A value of $\langle\Theta^{(r)}_{s\nabla\omega}(t)\rangle = \pi/4$ would mean that on average the two vectors are almost independent, and a value larger than $\pi/4$ means that they are preferentially perpendicular to each other. Figure 5(a) shows that the average angle, or the degree of misalignment, between the vorticity gradient and the stretching direction of the strain at an earlier time increases with the time lag and reaches a maximum at $t > 0$, similar to vortex stretching in 3D and energy flux in 2D [29,36,37]. On the other hand, unlike vortex stretching in 3D, where the time scales of the evolution for different length scales depend on r, Figure 5(a) shows that the temporal evolutions of VGS at different length scales all have the same time scale, $t \approx 0.35\tau_F$, where $\tau_F \equiv \beta^{-1/3}$ [31]. This occurs because the characteristic time scales associated with all length scales in the direct enstrophy cascade range are the same, $\tau(r) \sim \omega'^{-1} \sim \beta^{-1/3}$, a feature of 2D turbulence [5]. Figure 5(a) thus represents direct experimental evidence demonstrating this single time scale for all length scales in the direct enstrophy cascade range. The evolution of the PDF of $\Theta^{r}_{s\nabla\omega}(t)$ for the scale $r = 0.8M$, which is well into the direct enstrophy cascade range, is shown in Fig. 5(b). We observe that indeed the vorticity gradient responds to the strain field and tends to be perpendicular to the stretching direction at earlier times. In the eigenframe of the earlier strain, the

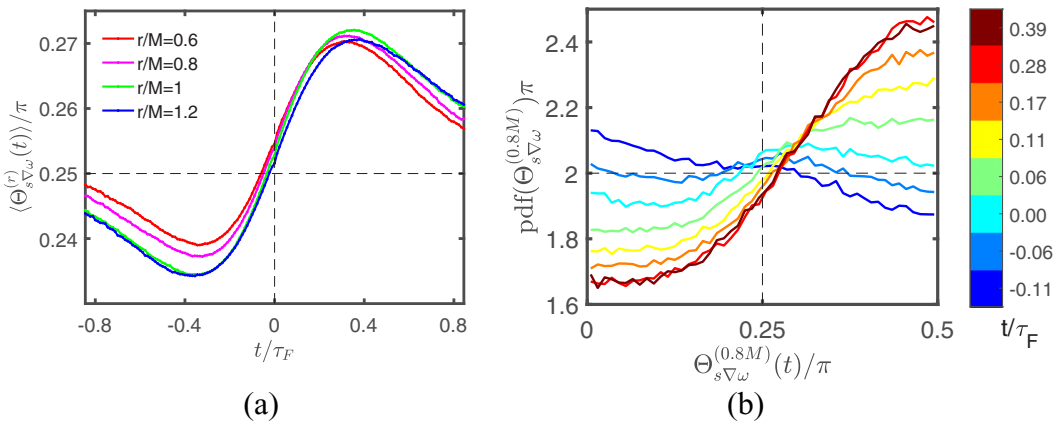

FIG. 5. Statistics of the angle $\Theta^{(r)}_{s\nabla\omega}(t)$ between $\mathbf{e}^{(r)}_s(0)$ and $\mathbf{e}^{(r)}_{\nabla\omega}(t)$ with the time lag t for different scales r in the direct cascade range. (a) The average angle $\langle\Theta^{(r)}_{s\nabla\omega}(t)\rangle$ as a function of time for different length scales r. The average angle is larger than $\pi/4$ after $t \approx 0$, which indicates preferential misalignment between the vorticity gradient and the stretching direction. (b) PDFs of the angle $\Theta^{(r)}_{s\nabla\omega}(t)$ at different time lags t for the length scale $r = 0.8M$, which is well into the direct cascade range. The color of the curves indicates the time lag t, as shown by the colorbar. At $t/\tau_F \approx 0.35$, the PDF peaks at nearly $\pi/2$, which indicates strong perpendicularity between the vorticity gradient direction and the stretching direction of the strain (or equivalently strong alignment between the vorticity gradient and the compression direction).

preferential misalignment increases significantly with time. For other scales r in the direct cascade range, the evolution of the PDF is similar.

We also examined the rate of evolution of the alignment, following an analysis similar to that done for vortex stretching in 3D [37]. We make an analogy between the evolution equation for the filtered vorticity gradient in the direct cascade range and the true vorticity gradient in inviscid flows, i.e.,

$$\frac{D(\nabla\omega)^{(r)}_j}{Dt} = -A^{(r)}_{ij}(\nabla\omega)^{(r)}_i, \tag{5}$$

where $\mathbf{A}^{(r)} = \nabla\mathbf{u}^{(r)}$ is the gradient of the filtered velocity field, which includes the symmetric part $\mathbf{s}^{(r)} = [\mathbf{A}^{(r)} + \mathbf{A}^{(r)T}]/2$ and the antisymmetric part $\mathbf{\Omega}^{(r)} = [\mathbf{A}^{(r)} - \mathbf{A}^{(r)T}]/2$. This equation leads to the evolution of the direction of the filtered vorticity gradient as

$$\begin{aligned}\frac{D\mathbf{e}^{(r)}_{\nabla\omega}}{Dt} &= -\mathbf{A}^{(r)T}\cdot\mathbf{e}^{(r)}_{\nabla\omega} + \left[\mathbf{e}^{(r)}_{\nabla\omega}\cdot\mathbf{A}^{(r)T}\cdot\mathbf{e}^{(r)}_{\nabla\omega}\right]\mathbf{e}^{(r)}_{\nabla\omega} \\ &= -\mathbf{s}^{(r)}\cdot\mathbf{e}^{(r)}_{\nabla\omega} + \mathbf{\Omega}^{(r)}\cdot\mathbf{e}^{(r)}_{\nabla\omega} + \left[\mathbf{e}^{(r)}_{\nabla\omega}\cdot\mathbf{s}^{(r)}\cdot\mathbf{e}^{(r)}_{\nabla\omega}\right]\mathbf{e}^{(r)}_{\nabla\omega},\end{aligned} \tag{6}$$

in which we have used $\mathbf{A}^{(r)T} = \mathbf{s}^{(r)} + \mathbf{\Omega}^{(r)T} = \mathbf{s}^{(r)} - \mathbf{\Omega}^{(r)}$ and $\mathbf{e}^{(r)}_{\nabla\omega}\cdot\mathbf{\Omega}^{(r)}\cdot\mathbf{e}^{(r)}_{\nabla\omega} = 0$ because the dyad $\mathbf{e}^{(r)}_{\nabla\omega}\mathbf{e}^{(r)}_{\nabla\omega}$ is symmetric but $\mathbf{\Omega}^{(r)}$ is antisymmetric. We now study how $\mathbf{e}^{(r)}_{\nabla\omega}$, the direction of the gradient of the filtered vorticity, evolves in the eigenframe spanned by $\mathbf{e}_i(0)$, the eigenvectors of the filtered rate of strain tensor at some given time, $\mathbf{s}^{(r)}(0)$. We note that this reference frame, $\mathbf{e}_i(0)$, is fixed in space, not the one embedded with the rate of strain $\mathbf{s}^{(r)}(t)$ and thus changing with time. Also note that in this frame, Eq. (6) holds only at the time $t = 0$. We project $\mathbf{e}^{(r)}_{\nabla\omega}$ onto the eigenvectors as $\mathbf{e}^{(r)}_{\nabla\omega} = c_1\mathbf{e}_1(0) + c_2\mathbf{e}_2(0)$, where $\mathbf{e}_1(0)$ and $\mathbf{e}_2(0)$ are the eigenvectors of $\mathbf{s}^{(r)}(0)$ corresponding to the eigenvalues $\lambda_1 = \lambda^{(r)}_s(0)$ and $\lambda_2 = -\lambda^{(r)}_s(0)$, respectively, and $c_i \equiv \mathbf{e}^{(r)}_{\nabla\omega}\cdot\mathbf{e}_i(0)$. Equation (6) then

gives the evolution of c_i as

$$\left.\frac{Dc_i}{Dt}\right|_{t=0} = -c_i\left(\lambda_i - \sum_{j=1}^{2}\lambda_j c_j^2\right) + \mathbf{e}_i(0)\cdot\left(\mathbf{\Omega}^{(r)}\cdot\mathbf{e}_{\nabla\omega}^{(r)}\right). \tag{7}$$

Because $\mathbf{\Omega}^{(r)}\cdot\mathbf{e}_{\nabla\omega}^{(r)} = \frac{1}{2}\boldsymbol{\omega}^{(r)}\times\mathbf{e}_{\nabla\omega}^{(r)}$, the last term in the equation above can be written as

$$\mathbf{e}_i(0)\cdot(\mathbf{\Omega}^{(r)}\cdot\mathbf{e}_{\nabla\omega}^{(r)}) = \frac{1}{2}\mathbf{e}_i(0)\cdot(\boldsymbol{\omega}^{(r)}\times\mathbf{e}_{\nabla\omega}^{(r)}) = \frac{1}{2}\omega^{(r)}\,\mathbf{e}_i(0)\cdot(\mathbf{e}_{\omega}^{(r)}\times\mathbf{e}_{\nabla\omega}^{(r)}) = \frac{1}{2}\omega^{(r)}\,\mathbf{e}_{\nabla\omega}^{(r)}\cdot(\mathbf{e}_i(0)\times\mathbf{e}_{\omega}^{(r)}),$$

where $\mathbf{e}_{\omega}^{(r)} = \mathbf{e}_3(0)$ is the unit vector normal to the flow plane. Noting that $\mathbf{e}_2(0)\times\mathbf{e}_{\omega}^{(r)} = -\mathbf{e}_1(0)$ and $\mathbf{e}_1(0)\times\mathbf{e}_{\omega}^{(r)} = -\mathbf{e}_2(0)$, Equation (7) for $i = 1$ and 2 becomes

$$\left.\frac{Dc_1}{Dt}\right|_{t=0} = -2\lambda_s^{(r)}c_1c_2^2 - \frac{1}{2}\omega^{(r)}c_2 \tag{8}$$

and

$$\left.\frac{Dc_2}{Dt}\right|_{t=0} = 2\lambda_s^{(r)}c_1^2c_2 + \frac{1}{2}\omega^{(r)}c_1. \tag{9}$$

The evolution of the angle $\Theta_{s\nabla\omega}^{(r)}$ between $\mathbf{s}^{(r)}$ and $(\nabla\omega)^{(r)}$ can be derived from Eqs. (8) and (9) by noting that $\tan\Theta_{s\nabla\omega}^{(r)} = c_2/c_1$. The result is simply

$$\left.\frac{D\Theta_{s\nabla\omega}^{(r)}}{Dt}\right|_{t=0} = \lambda_s^{(r)}\sin 2\Theta_{s\nabla\omega}^{(r)} + \frac{1}{2}\omega^{(r)}. \tag{10}$$

This equation shows explicitly that the vorticity itself affects the evolution of the angle between the stretching direction and the vorticity gradient, $\Theta_{s\nabla\omega}^{(r)}$, which differs from the alignment between vorticity and the stretching direction in 3D flows where the alignment process is determined by the rate of strain [37] because vorticity by itself cannot change the direction of the vorticity vector.

On the other hand, we are interested in the change of the average angle, $\langle\Theta_{s\nabla\omega}^{(r)}\rangle$, which evolves as

$$\left.\frac{D\langle\Theta_{s\nabla\omega}^{(r)}\rangle}{Dt}\right|_{t=0} = \langle\lambda_s^{(r)}\sin 2\Theta_{s\nabla\omega}^{(r)}\rangle + \frac{1}{2}\langle\omega^{(r)}\rangle. \tag{11}$$

The last term in this equation should vanish due to symmetry considerations: there is no net rotation of the flow, as in the case of the turbulence generated behind the grid in the soap film. Therefore, the change of the ensemble-averaged angle is also determined by the rate of strain, which means that although vorticity affects the evolution of the direction of each individual vorticity gradient, its effect vanishes when we average over a large sample. This is confirmed by the experimental data: the values of $\langle\omega^{(r)}\rangle/\langle\lambda_s^{(r)}\sin 2\Theta_{s\nabla\omega}^{(r)}\rangle$ are between 3–5% for the range of r that we investigated.

In Fig. 6, we compare the slope $D\langle\Theta_{s\nabla\omega}^{(r)}\rangle/Dt$ at $t = 0$ that we extract from data shown in Fig. 5(a) with the values of $\langle\lambda_s^{(r)}\sin 2\Theta_{s\nabla\omega}^{(r)}\rangle$, the right-hand side of Eq. (11), for the length scales we measured. The slope $D\langle\Theta_{s\nabla\omega}^{(r)}\rangle/Dt$ at $t = 0$ for different scales is nearly the same, which is another manifestation of the single time scale in the direct cascade range that we have seen before. The values of $\langle\lambda_s^{(r)}\sin 2\Theta_{s\nabla\omega}^{(r)}\rangle$ are, however, larger than the slopes at all scales, but the difference decreases when the scale increases. For flows with larger direct cascade ranges, we expect that Eq. (11) will give a better prediction of the evolution of the angle $\langle\Theta_{s\nabla\omega}^{(r)}\rangle$. The discrepancy is likely due to the neglect of viscous effects, which will on average resist the action of the strain in Eq. (5) and hence slow down the alignment compared to that given by the strain field alone, as shown by Eq. (11). As the scale increases, the effects of viscosity decrease and the right-hand side of Eq. (11) agrees better with the measured slope. It would be interesting to compare our results with a 2D DNS

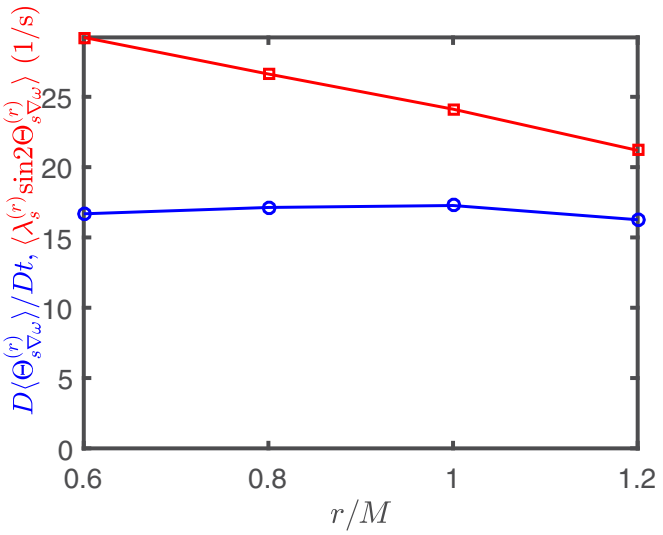

FIG. 6. The evolution of the average angle $\langle\Theta^{(r)}_{s\nabla\omega}\rangle$ at $t = 0$ for several scales r. Blue circles are slopes extracted from the data shown in Fig. 5(a) by finite difference. Red squares are the effect due to stretching $\langle\lambda^{(r)}_s \sin 2\Theta^{(r)}_{s\nabla\omega}\rangle$.

with a robust forward cascade, from which the contribution from each term could be obtained with high accuracy.

V. CONCLUSION

In summary, by performing particle tracking measurements in a soap-film flow, we investigated the stretching of vorticity gradients in 2D turbulence. From instantaneous flow fields, we observed that the vorticity gradient is preferentially perpendicular to the stretching direction of the strain, a manifestation of VGS, and there is strong correlation between VGS and enstrophy flux. Moreover, by investigating the alignment between the vorticity gradient and the eigendirection of the rate of strain tensor along Lagrangian trajectories, we observed that the strain rate leads the vorticity gradient in time, i.e., the vorticity gradient responds to the strain and tends to be antialigned with the stretching direction of the strain at earlier times. For all scales in the direct enstrophy cascade range, the angle between the vorticity and the strain evolves on the same time scale, which is clear experimental evidence that there is only a single time scale in the direct enstrophy cascade range [5,8].

Finally, we note that it has been suggested that the inverse energy cascade in 2D turbulence is realized through vortex thinning [26,27], and a correlation between instantaneous straining regions and scale-to-scale energy flux has been indeed observed [33]. Vortex thinning refers to the elongation and thinning of small-scale vortices by large-scale strain, which causes velocity differences at larger scales to increase [26,27]. Therefore, we argue that vortex thinning and VGS are in fact the same physical phenomenon. It is interesting that the same physical process is associated with both the inverse energy cascade to larger scales and the direct enstrophy cascade to smaller scales [5].

ACKNOWLEDGMENTS

Z.Z. and H.X. are grateful for financial support from Tsinghua University. L.F. and N.T.O. acknowledge support from the U.S. National Science Foundation under Grants No. CMMI-1563489 and No. CBET-1706950. We are grateful to the anonymous referees for their constructive comments that helped to improve the manuscript.

[1] G. I. Taylor, Production and dissipation of vorticity in a turbulent fluid, Proc. R. Soc. London, Ser. A **164**, 476 (1938).
[2] T. Tennekes and J. L. Lumley, *A First Course in Turbulence* (MIT, Cambridge, MA, 1972).
[3] U. Frisch, *Turbulence: The Legacy of A. N. Kolmogorov* (Cambridge University, Cambridge, England, 1995).
[4] S. B. Pope, *Turbulent Flows* (Cambridge University, Cambridge, England, 2000).
[5] P. Davidson, *Turbulence: An Introduction for Scientists and Engineers* (Oxford University, Oxford, 2015).
[6] R. H. Kraichnan, Inertial ranges in two-dimensional turbulence, Phys. Fluids **10**, 1417 (1967).
[7] G. Boffetta and R. E. Ecke, Two-dimensional turbulence, Annu. Rev. Fluid Mech. **44**, 427 (2012).
[8] G. K. Batchelor, Computation of the energy spectrum in homogeneous two-dimensional turbulence, Phys. Fluids **12**, II-233 (1969).
[9] B. K. Martin, X. L. Wu, W. I. Goldburg, and M. A. Rutgers, Spectra of Decaying Turbulence in a Soap Film, Phys. Rev. Lett. **80**, 3964 (1998).
[10] G. Boffetta, Energy and enstrophy fluxes in the double cascade of two-dimensional turbulence, J. Fluid Mech. **589**, 253 (2007).
[11] G. Falkovich, G. Boffetta, M. Shats, and A. S. Lanotte, Introduction to focus issue: Two-dimensional turbulence, Phys. Fluids **29**, 110901 (2017).
[12] S. Chen, R. E. Ecke, G. L. Eyink, X. Wang, and Z. Xiao, Physical Mechanism of the Two-Dimensional Enstrophy Cascade, Phys. Rev. Lett. **91**, 214501 (2003).
[13] G. Lapeyre, P. Klein, and B. L. Hua, Does the tracer gradient vector align with the strain eigenvectors in 2D turbulence?, Phys. Fluids **11**, 3729 (1999).
[14] G. Lapeyre, B. L. Hua, and P. Klein, Dynamics of the orientation of active and passive scalars in two-dimensional turbulence, Phys. Fluids **13**, 251 (2001).
[15] T. Dubos and A. Babiano, Comparing the two-dimensional cascades of vorticity and a passive scalar, J. Fluid Mech. **492**, 131 (2003).
[16] A. Tsinober, *An Informal Conceptual Introduction to Turbulence* (Springer, Berlin, 2009).
[17] Y. Couder, J. M. Chomaz, and M. Rabaud, On the hydrodynamics of soap films, Phys. D **37**, 384 (1989).
[18] M. A. Rutgers, X. L. Wu, and W. B. Daniel, Conducting fluid dynamics experiments with vertically falling soap films, Rev. Sci. Instrum. **72**, 3025 (2001).
[19] H. Kellay and W. I. Goldburg, Two-dimensional turbulence: A review of some recent experiments, Rep. Prog. Phys. **65**, 845 (2002).
[20] P. Vorobieff and R. E. Ecke, Cylinder wakes in flowing soap films, Phys. Rev. E **60**, 2953 (1999).
[21] N. T. Ouellette, H. Xu, and E. Bodenschatz, A quantitative study of three-dimensional Lagrangian particle tracking algorithms, Exp. Fluids **40**, 301 (2006).
[22] H. Xu, Tracking Lagrangian trajectories in position-velocity space, Meas. Sci. Technol. **19**, 075105 (2008).
[23] R. Ni, S. Kramel, N. T. Ouellette, and G. A. Voth, Measurements of the coupling between the tumbling of rods and the velocity gradient tensor in turbulence, J. Fluid Mech. **766**, 202 (2015).
[24] G. L. Eyink, Local energy flux and the refined similarity hypothesis, J. Stat. Phys. **78**, 335 (1995).
[25] M. K. Rivera, W. B. Daniel, S. Y. Chen, and R. E. Ecke, Energy and Enstrophy Transfer in Decaying Two-Dimensional Turbulence, Phys. Rev. Lett. **90**, 104502 (2003).
[26] S. Chen, R. E. Ecke, G. L. Eyink, M. Rivera, M. Wan, and Z. Xiao, Physical Mechanism of the Two-Dimensional Inverse Energy Cascade, Phys. Rev. Lett. **96**, 084502 (2006).
[27] Z. Xiao, M. Wan, S. Chen, and G. L. Eyink, Physical mechanism of the inverse energy cascade of two-dimensional turbulence: A numerical investigation, J. Fluid Mech. **619**, 1 (2009).
[28] Y. Liao and N. T. Ouellette, Spatial structure of spectral transport in two-dimensional flow, J. Fluid Mech. **725**, 281 (2013).
[29] L. Fang and N. T. Ouellette, Advection and the Efficiency of Spectral Energy Transfer in Two-Dimensional Turbulence, Phys. Rev. Lett. **117**, 104501 (2016).
[30] J. G. Ballouz and N. T. Ouellette, Tensor geometry in the turbulent cascade, J. Fluid Mech. **835**, 1048 (2018).

[31] P. Vorobieff, M. Rivera, and R. E. Ecke, Soap film flows: Statistics of two-dimensional turbulence, Phys. Fluids **11**, 2167 (1999).
[32] M. K. Rivera, H. Aluie, and R. E. Ecke, The direct enstrophy cascade of two-dimensional soap film flows, Phys. Fluids **26**, 055105 (2014).
[33] Y. Liao and N. T. Ouellette, Correlations between the instantaneous velocity gradient and the evolution of scale-to-scale fluxes in two-dimensional flow, Phys. Rev. E **92**, 033017 (2015).
[34] R. M. Kerr, Histograms of Helicity and Strain in Numerical Turbulence, Phys. Rev. Lett. **59**, 783 (1987).
[35] A. Tsinober, E. Kit, and T. Dracos, Experimental investigation of the field of velocity gradients in turbulent flows, J. Fluid Mech. **242**, 169 (1992).
[36] H. Xu, A. Pumir, and E. Bodenschatz, The pirouette effect in turbulent flows, Nat. Phys. **7**, 709 (2011).
[37] A. Pumir, E. Bodenschatz, and H. Xu, Tetrahedron deformation and alignment of perceived vorticity and strain in a turbulent flow, Phys. Fluids **25**, 035101 (2013).
[38] R. Ni, N. T. Ouellette, and G. A. Voth, Alignment of vorticity and rods with Lagrangian fluid stretching in turbulence, J. Fluid Mech. **743**, R3 (2014).